



Article

# CuMo<sub>x</sub>W<sub>(1-x)</sub>O<sub>4</sub> Solid Solution Display Visible Light Photoreduction of CO<sub>2</sub> to CH<sub>3</sub>OH Coupling with Oxidation of Amine to Imine

Chao Luo <sup>1</sup>, Tian Yang <sup>2</sup>, Qianfei Huang <sup>3</sup>, Xian Liu <sup>2</sup>, Huan Ling <sup>1</sup>, Yuxin Zhu <sup>1</sup>, Guoming Xia <sup>1</sup>, Wennan Zou <sup>1,\*</sup> and Hongming Wang <sup>1,\*</sup>

<sup>1</sup> Institute for Advanced Study, Nanchang University, Nanchang 330031, China; luochao@ncu.edu.cn (C.L.); huanling\_ncu@126.com (H.L.); ncu\_zhuyuxin@163.com (Y.Z.); gmxia\_ncu@126.com (G.X.)

<sup>2</sup> College of Chemistry, Nanchang University, Nanchang 330031, China; yangtian\_92@163.com (T.Y.); lzhnxylx@163.com (X.L.)

<sup>3</sup> School of Information Engineering, Jiangxi Modern Polytechnic College, Nanchang 330095, China; huangqianfei1015@hotmail.com

\* Correspondence: zouwn@ncu.edu.cn (W.Z.); hongmingwang@ncu.edu.cn (H.W.)

Received: 16 June 2020; Accepted: 28 June 2020; Published: 3 July 2020



**Abstract:** The photoreduction of carbon dioxide (CO<sub>2</sub>) to valuable fuels is a promising strategy for the prevention of rising atmospheric levels of CO<sub>2</sub> and the depletion of fossil fuel reserves. However, most reported photocatalysts are only active in the ultraviolet region, which necessitates co-catalysts and sacrificial agents in the reaction systems, leading to an unsatisfied economy of the process in energy and atoms. In this research, a CuMo<sub>x</sub>W<sub>(1-x)</sub>O<sub>4</sub> solid solution was synthesized, characterized, and tested for the photocatalytic reduction of CO<sub>2</sub> in the presence of amines. The results revealed that the yield of CH<sub>3</sub>OH from CO<sub>2</sub> was 1017.7 μmol/g under 24 h visible light irradiation using CuW<sub>0.7</sub>Mo<sub>0.3</sub>O<sub>4</sub> (x = 0.7) as the catalyst. This was associated with the maximum conversion (82.1%) of benzylamine to *N*-benzylidene benzylamine with high selectivity (>99%). These results give new insight into the photocatalytic reduction of CO<sub>2</sub> for valuable chemical products in an economic way.

**Keywords:** photocatalysis; visible light; solid solution; reduction of CO<sub>2</sub>

## 1. Introduction

For energy conservation and environmental protection, direct conversion of CO<sub>2</sub> into a source of carbon fuels is an ideal solution [1–7]. Among the different technologies, solar photocatalytic conversion of CO<sub>2</sub> is the most promising because it only needs sunlight at room temperature and ambient pressure, which is clean, safe, and abundant [8–14]. As such, the development of an efficient photocatalyst under sunlight irradiation is attractive and has become a research hotspot. Over past decades, various photocatalytic materials have been analyzed: TiO<sub>2</sub> [15–17], CdS [18,19], Bi<sub>2</sub>O<sub>3</sub> [20,21], CeO<sub>2</sub> [22,23], and Bi<sub>2</sub>WO<sub>6</sub> [24–26]. Their well-designed heterostructures have been examined for reduction of CO<sub>2</sub> to fuels, such as CO [27–29], CH<sub>4</sub> [30–32], CH<sub>3</sub>OH [33,34], and C<sub>2</sub>H<sub>6</sub> [35,36], but the overall photoconversion efficiency and product selectivity is still unsatisfactory and requires further promotion for practical applications.

It has been confirmed that forming a solid solution between semiconductors is an excellent method in the development of visible light-driven photocatalysts for sensitive photoreduction of CO<sub>2</sub> [37–40] and is widely applied in photocatalytic water splitting and pollutant degradation, while exhibiting better performance than single components comprising the solid solution [41–46]. Taking this into account, a series of solid solution photocatalysts, such as BiOBr<sub>x</sub>Cl<sub>1-x</sub> [47], Zn<sub>x</sub>Cd<sub>1-x</sub>S [48], GaN:ZnO [49], and zinc gallogermanate [39], have been synthesized and examined for CO<sub>2</sub> reduction under visible light

irradiations. Very recently, Ling and colleagues [50] demonstrated that  $\text{Cu}_x\text{Ag}_y\text{In}_z\text{Zn}_k\text{S}$  solid solutions customized with  $\text{RuO}_2$  or a  $\text{Rh}_{1.32}\text{Cr}_{0.66}\text{O}_3$  co-catalyst showed high photocatalytic activity for the reduction of  $\text{CO}_2$  into  $\text{CH}_3\text{OH}$  with a yield up to  $118.5 \mu\text{mol g}^{-1} \text{h}^{-1}$  under visible light irradiation. Liang's group [51] reported that a N-doped, graphene-functionalized  $\text{Zn}_{1.231}\text{Ge}_{0.689}\text{N}_{1.218}\text{O}_{0.782}$  solid solution exhibited high photocatalytic activity for the evolution of  $\text{CH}_4$  from the photocatalytic reaction of  $\text{CO}_2$  and  $\text{H}_2\text{O}$ , coupled with oxidation of benzyl alcohol under visible light irradiation.

Since the pioneering work of Benko,  $\text{CuWO}_4$  has been confirmed as a promising photoanode material for photoelectrochemical (PEC) splitting water, with a narrower band gap of 2.3 eV that allows for the use of visible light and enhanced stability in neutral and moderate to basic pH [52,53]. In this work, a  $\text{CuMo}_x\text{W}_{(1-x)}\text{O}_4$  solid solution was synthesized by a facile hydrothermal method and then examined for the photocatalytic reduction of  $\text{CO}_2$  under visible light irradiation without the addition of any co-catalysts and sacrificed reagents in the system. In this process,  $\text{CO}_2$  was reduced to  $\text{CH}_3\text{OH}$  by photo-induced electrons, while amine was selected as the "hydrogen-donor" to capture the photogenerated holes. Then, the amine was converted into imine, resulting in good energy and atomic economies.

## 2. Experimental

### 2.1. General

All chemicals and solvents were purchased from commercial suppliers and used as received unless explicitly stated. Using tetramethylsilane (TMS) as an internal standard,  $^1\text{H}$  nuclear magnetic resonance (NMR) and  $^{13}\text{C}$  NMR spectra were measured on a Bruker AVANCE 400 spectrometer (Basel, Switzerland) in  $\text{CDCl}_3$ . X-ray diffraction (XRD) data were collected on a D8 diffractometer from Bruker Instruments (Basel, Switzerland), utilizing  $\text{Cu K}\alpha$  radiation at a scan rate of  $0.05 \text{ s}^{-1}$ . The scanning electron microscopy (SEM) images were obtained by a Quanta 200F FEI (Los Angeles, USA). Transmission electron microscopy (TEM) analysis was carried out on a JEM-2100 (TEM) (Okinawa, Japan), and energy dispersive X-ray spectra (EDX) were obtained at an accelerating voltage of 200 kV. X-ray photoelectron spectroscopy (XPS) data were performed with a Thermo Scientific (New York, USA) ESCALAB250Xi XPS spectrometer with  $\text{Al K}\alpha$  at 500 eV. The ultraviolet-visible (UV-Vis) DRS spectra of photocatalysts were conducted using a Cary 60 UV-vis spectrophotometer (London, Europe) with  $\text{BaSO}_4$  as a reference. Photoluminescence (PL) characterizations were carried out on a FluoroMax-4 spectrometer (London, Europe), using a  $\lambda_{\text{ex}} = 320 \text{ nm}$  light source. Gas chromatography (GC) product analysis was performed on a flame ionization detector. The composition of liquid products was analyzed by GC-MS (Beijing, China) with a HP-5 capillary column ( $30 \text{ m} \times 0.25 \text{ mm} \times 0.25 \text{ mm}$ ).

### 2.2. The Preparation of Solid Solution Photocatalysts

A series of  $\text{CuMo}_x\text{W}_{(1-x)}\text{O}_4$  solid solution photocatalysts was prepared by a typical hydrothermal synthesis method, in which X is defined as the molar ratio of  $\text{Mo}/(\text{Mo} + \text{W})$ . Setting the preparation of  $\text{CuMo}_{0.1}\text{W}_{0.9}\text{O}_4$  ( $X = 0.1$ ) as an example: 10 mmol  $\text{Cu}(\text{NO}_3)_2 \cdot 3\text{H}_2\text{O}$  was dissolved in 250 mL distilled water as precursor solution A. Onethousandth of a mol of  $\text{NaMoO}_4 \cdot 2\text{H}_2\text{O}$  and 9.0 mmol  $\text{NaWO}_4 \cdot 2\text{H}_2\text{O}$  were dissolved in 250 mL distilled water as precursor solution B. Precursor solution A was added dropwise to precursor solution B under a strong stirring condition in 30 min, during which the mixtures turned blue-green and more suspended substance appeared. After the addition, the suspended substance (about 80 mL) was then transferred into a 100 mL autoclave and heated at  $180 \text{ }^\circ\text{C}$  for 24 h. After cooling to room temperature, the obtained product was then filtered and washed with distilled water and anhydrous alcohol several times and then dried in a vacuum at  $80 \text{ }^\circ\text{C}$  for 10 h. The other photocatalysts could be easily prepared in the same way by adjusting the molar ratio:  $\text{Mo}/(\text{Mo} + \text{W})$ .

### 2.3. Photocatalytic Reduction of CO<sub>2</sub>

Photocatalytic reactions were carried out in 40 mL anhydrous acetonitrile with 0.06 g corresponding to the photocatalyst and 1 mmol benzylamine (purified by distilled before using) in an 80 mL self-made quartz reactor at 0.5 MPa CO<sub>2</sub> partial pressure. Before the reaction, the reactor was evacuated with high-purity dry CO<sub>2</sub> gas and blown through several times to remove lesser quantities of oxygen, and then it was tightly closed. Before illumination, the reaction system was stirred under darkness to prompt CO<sub>2</sub> adsorption and desorption equilibrium after blowing CO<sub>2</sub> for 30 min. Then, a Xe lamp (300 W) with a 420 nm cut-off filter was turned on as the light source for the photocatalytic reactions. During the processes, the reaction temperature was maintained at room temperature with a circulating cool water bath. After the reactions were complete, the products were immediately analyzed by GC (Figure S1), <sup>1</sup>H NMR (Figure S2), and MS (Figure S3). Detailed calculations of methanol yield, conversion rate of benzylamine, and selectivity of N-benzylidenebenzylamine are shown in the Supporting Information.

## 3. Results and Discussion

### 3.1. Catalyst Characterization

#### 3.1.1. XRD and EDX Analysis

To reveal the phase structure of various photocatalysts prepared by the hydrothermal method, XRD patterns were recorded and shown in Figure 1. The CuMo<sub>x</sub>W<sub>(1-x)</sub>O<sub>4</sub> photocatalysts were formed in two different crystalline structures, depending on their chemical composition. For  $x \leq 0.7$ , the XRD patterns exhibit several broad diffraction peaks with low intensity, suggesting that these photocatalysts were in a poor crystalline state. Moreover, the patterns of these materials are in good agreement with the standard spectrum of CuWO<sub>4</sub>·H<sub>2</sub>O [54,55] (JCPDS no.: 33-0503). For  $x \geq 0.8$ , several sharp diffraction peaks appeared and intensified, indicating that these photocatalysts are in a good crystalline state.  $2\theta$  values of 20.4, 21.4, 24.9, 25.3, 25.4, and 25.9 correspond to the Cu<sub>3</sub>(MoO<sub>4</sub>)<sub>2</sub>(OH)<sub>2</sub> of the (021) (101), (121), (130), (040), and (111) faces, respectively, which is in agreement with the reported values [56]. It can be interpreted that the increased Mo content had some effects on the crystal structure of these photocatalysts in the system [56]. Furthermore, the EDX analysis results of the sample are shown in Figure 2 and Table 1. The Mo content in the reaction system gradually increased with increasing  $x$  values, and the sample changed from CuWO<sub>4</sub>·H<sub>2</sub>O to Cu<sub>3</sub>(MoO<sub>4</sub>)<sub>2</sub>(OH)<sub>2</sub>. In addition, the XPS spectra of the samples were obtained (Figure S5), which clearly indicate that the Cu and W atoms exist in the form of Cu<sup>2+</sup> and W<sup>6+</sup>, respectively.

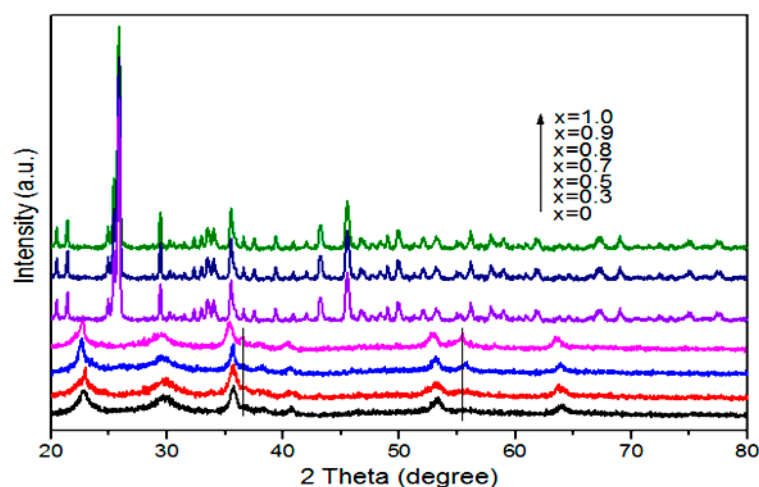
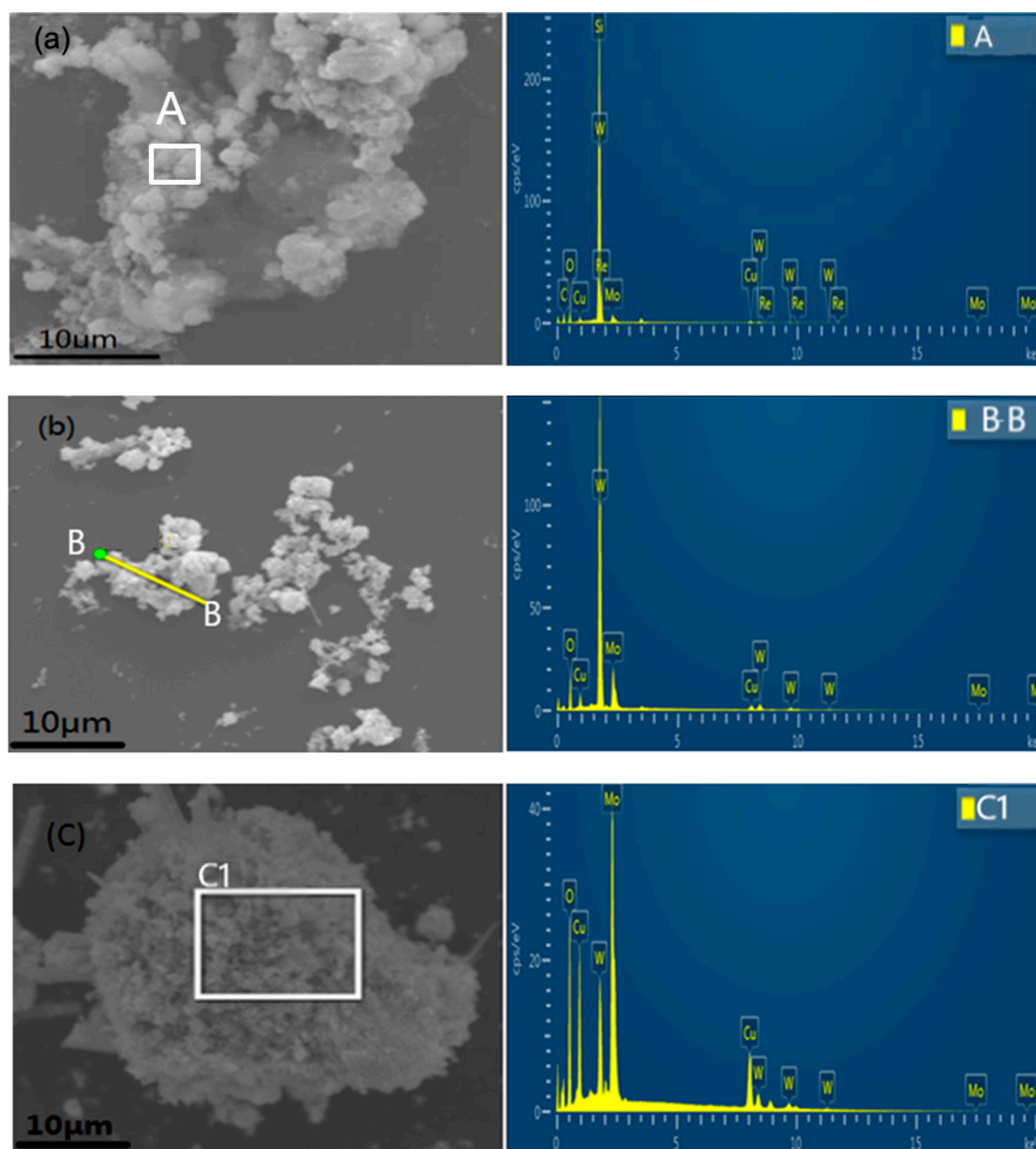


Figure 1. XRD patterns of nanoparticles prepared by hydrothermal method at 180 °C.



**Figure 2.** Energy dispersive X-ray spectra (EDX) spectra of (a)  $\text{CuMo}_{0.5}\text{W}_{0.5}\text{O}_4$  ( $x = 0.5$ ) and the plane (A), (b)  $\text{CuMo}_{0.7}\text{W}_{0.3}\text{O}_4$  ( $x = 0.7$ ) and the line (B-B), and (c)  $\text{CuMo}_{0.8}\text{W}_{0.2}\text{O}_4$  ( $x = 0.8$ ) and the plane (C1).

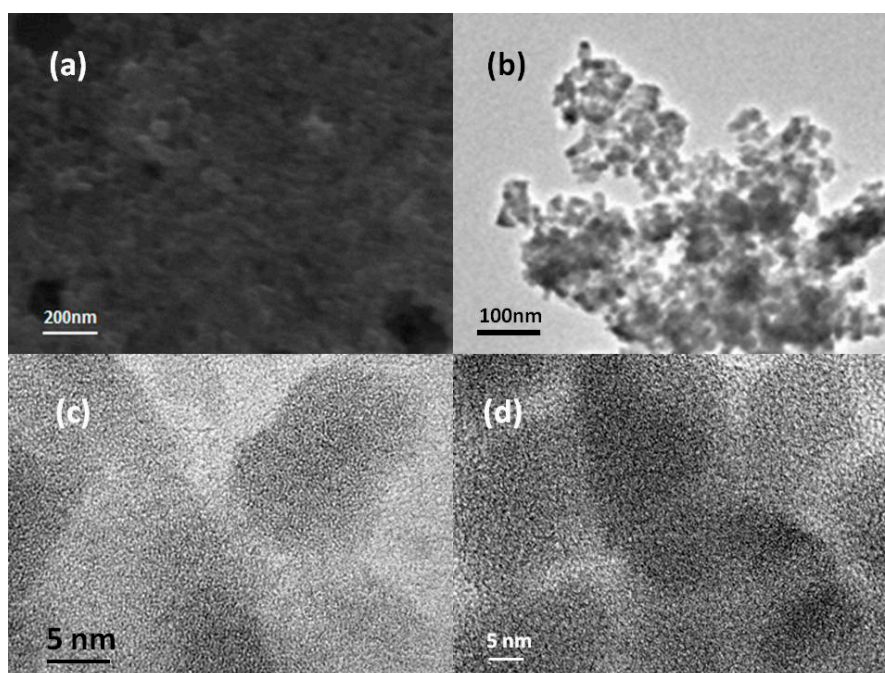
**Table 1.** Molar ratio of Cu:Mo:W.

Entry	The Value of x	The Ratio of Cu:Mo:W
1	0.5	1:0.12:0.97
2	0.7	1:0.23:1.05
3	0.8	1:0.76:0.13

### 3.1.2. SEM and TEM Analysis

Figure 3 shows the SEM and TEM micromorphology of the prepared samples. As seen in Figure 3a, the surface of the selected material prepared by the hydrothermal method was smooth and existed in globular particles. To observe the microstructure of the photocatalyst, the characterization of the photocatalyst ( $x = 0.7$ ) was carried out using TEM, and the average particle size was shown to be about 30 nm (Figure 3b). The high resolution transmission electron microscopy (HR-TEM) images of the

interfacial structure of the photocatalyst in different regions is shown in Figure 3c,d, indicating that the photocatalyst  $\text{CuMo}_{0.7}\text{W}_{0.3}\text{O}_4$  ( $x = 0.7$ ) prepared via hydrothermal method was amorphous because no obvious lattice stripes were observed in the photocatalyst.



**Figure 3.** (a) Scanning electron microscopy (SEM), (b) transmission electron microscopy (TEM), and (c), (d) high resolution transmission electron microscopy (HR-TEM) images of the  $\text{CuMo}_{0.7}\text{W}_{0.3}\text{O}_4$  ( $x = 0.7$ ) photocatalyst.

### 3.1.3. UV-Vis Absorption and PL Spectroscopy Analysis

UV-vis DRS spectra of the solid solutions were obtained, and the results are shown in Figure 4. The samples had a wide absorption with a wavelength range from 350 nm to 750 nm. A bathochromic shift absorption band (from 570 to 610 nm) was observed with increasing  $x$  values from 0 to 0.7. With a further increasing  $x$  value (from 0.8 to 1.0), a blue-shifted absorption band was observed from 620 nm to 580 nm. The different trends of the absorption bands can be verified via XRD spectra. When  $x \leq 0.7$ , these samples were in the form of  $\text{CuWO}_4 \cdot \text{H}_2\text{O}$ , but, when  $x > 0.7$ , they were in the form of  $\text{Cu}_3(\text{MoO}_4)_2(\text{OH})_2$ . Generally speaking, the absorption of the lower band is more easily disturbed by the introduction of Mo and W than the higher bands, which indicates that a charge transfer from  $\text{O}^{2-}$  to  $\text{Mo}^{6+}$  or  $\text{W}^{6+}$  contributes to the formation of the absorption band. This is consistent with a paper by Gaudon et al. [57,58].

As is well known, photoluminescence (PL) emission can be used to discover carrier transfer and recombination efficiency because it is caused by the recombination of photogenic carriers. Lower PL emission intensity suggests a lower recombination rate and exhibits higher photocatalytic activity for a photocatalyst [59,60], as shown in Figure 5, as the value of  $x$  increases from 0 to 0.7, the fluorescence intensity of the samples gradually weakens. This is mainly because the Mo content is gradually increasing, which inhibits the recombination of photogenerated charges and carriers, thereby improving the photocatalytic activity. The fluorescence intensity of the samples was gradually strengthened with further increases in  $x$  value (from 0.8 to 1.0). It is obvious that the PL emission spectra of samples can be divided into two categories (Figure 5). One type of spectrum was obtained for  $x$  values in the range of 0.8 to 1.0, showing strong PL emission with emission intensity increasing with increasing  $x$  value. Another emission intensity, lower than the former, was found when the  $x$  values were between 0 to 0.7.

All optical results revealed that the photocatalytic activity of  $\text{CuMo}_{0.7}\text{W}_{0.3}\text{O}_4$  ( $x = 0.7$ ) is optimal for the system.

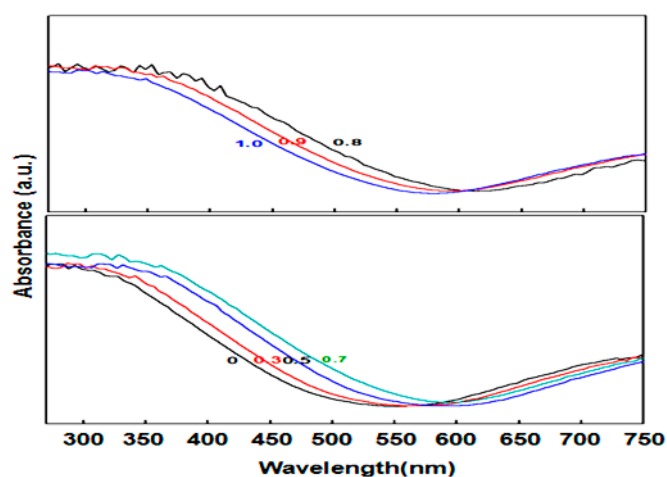


Figure 4. Ultraviolet-visible (UV-vis) diffuse reflectance spectra of different samples.

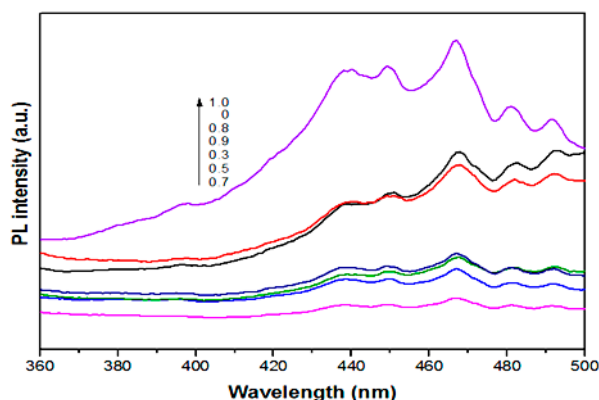


Figure 5. Photoluminescence emission spectra of different samples with excitation at 320 nm.

### 3.2. Photocatalytic Reduction of Carbon Dioxide Activity Measurement

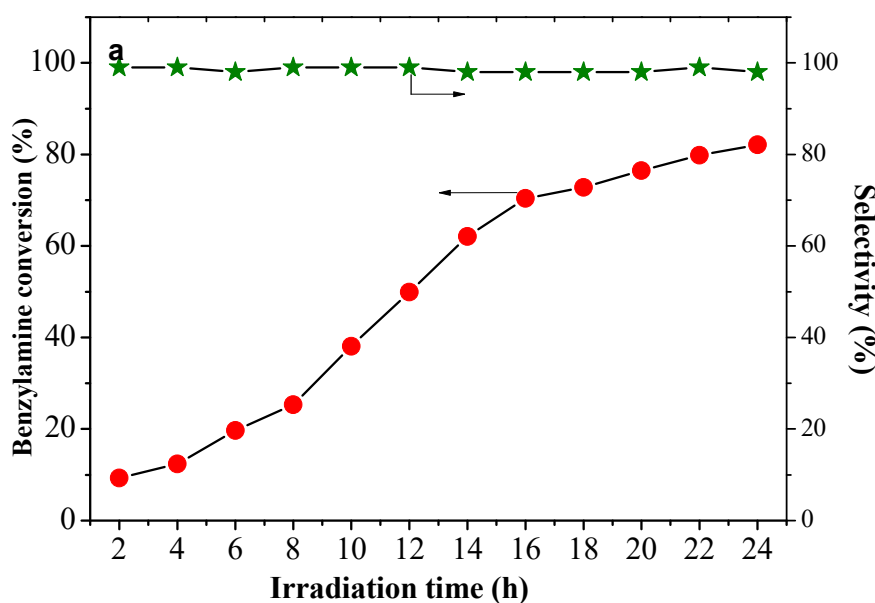
To investigate the performance of various photocatalysts prepared hydrothermally, the photocatalytic oxidation of amine to imine coupling with the reduction of  $\text{CO}_2$  to  $\text{CH}_3\text{OH}$  was carried out under visible light ( $\lambda > 420$  nm) irradiation and a 0.5 MPa  $\text{CO}_2$  pressure environment. The detailed results are shown in Table 2. These results prove that  $\text{CH}_3\text{OH}$  was selectively obtained from  $\text{CO}_2$ , and imine was produced from the oxidation of amine, which were further confirmed with GC, NMR, and MS analysis (Figures S1–S3). We found that benzylamine can be converted to *N*-benzylidene benzylamine with high selectivity (>99%) and  $\text{CO}_2$  can be converted to  $\text{CH}_3\text{OH}$  with good productivity after 12 h irradiation with photocatalysts. Moreover, the results suggested that  $\text{CuW}_{0.7}\text{Mo}_{0.3}\text{O}_4$  ( $x = 0.7$ ) was the optimum photocatalyst among the examined samples, which showed the highest conversion of benzylamine (57.2%) and high selectivity towards *N*-benzylidenebenzylamine (>99%) within 14 h irradiations (Table 2, entry 4), and received the highest productivity of  $\text{CH}_3\text{OH}$  up to 671.8  $\mu\text{mol/g}$ . These results are almost consistent with optical observations. Therefore, the  $\text{CuW}_{0.7}\text{Mo}_{0.3}\text{O}_4$  ( $x = 0.7$ ) was selected as the photocatalyst in the following experiments. In addition, the results of two blank reactions showed that the conversion of benzylamine was 7.1 and 91.3% in the absence of catalyst and in the presence of catalyst, respectively.

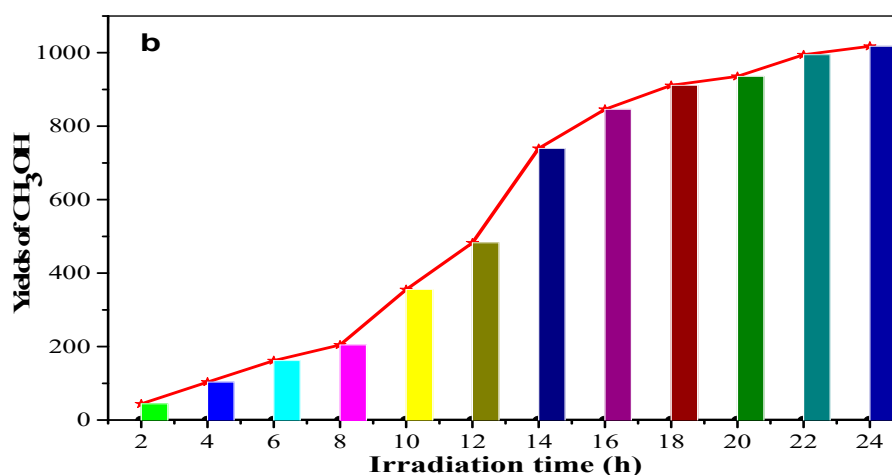
**Table 2.** Photocatalytic activity of different nanoparticles.

Entry	Catalyst	Gas	CH <sub>3</sub> OH ( $\mu\text{mol/g}$ )	Amine Conv. (%)	Imine Sel. (%)
	the Value of x				
1	0	CO <sub>2</sub>	296.9	29.5	>99
2	0.3	CO <sub>2</sub>	375.4	35.9	>99
3	0.5	CO <sub>2</sub>	571.2	48.3	>99
4	0.7	CO <sub>2</sub>	671.8	54.2	>99
5	0.8	CO <sub>2</sub>	509.9	45.7	>97
6	0.9	CO <sub>2</sub>	394.6	34.4	>99
7	1.0	CO <sub>2</sub>	249.3	23.1	>99
8 <sup>a</sup>	0.7	N <sub>2</sub>	–	2.1	–
9 <sup>b</sup>	–	CO <sub>2</sub>	–	1.7	–
10 <sup>c</sup>	0.7	CO <sub>2</sub>	51.7	9.5	>99
11 <sup>d</sup>	0.7	CO <sub>2</sub>	–	–	–
12 <sup>e</sup>	0.7	CO <sub>2</sub>	–	91.3	–
13 <sup>f</sup>	–	CO <sub>2</sub>	–	7.1	–

<sup>a</sup> 1 mmol benzylamine; 40 mL CH<sub>3</sub>CN, 60 mg photocatalyst; <sup>b</sup> without photocatalyst; <sup>c</sup> 40 mL benzylamine, without CH<sub>3</sub>CN; <sup>d</sup> 40 mL CH<sub>3</sub>CN, without benzylamine; <sup>e</sup> O<sub>2</sub>, <sup>f</sup> O<sub>2</sub>, without photocatalyst.

The time plot for the oxidation of benzylamine to the corresponding imine under 0.5 MPa of CO<sub>2</sub> on CuW<sub>0.7</sub>Mo<sub>0.3</sub>O<sub>4</sub> ( $x = 0.7$ ) is shown in Figure 6a,b. With prolonged irradiation time, the conversion of benzylamine was significantly enhanced, accompanied by an increased yield in CH<sub>3</sub>OH. As shown, the yield of CH<sub>3</sub>OH increased slightly within 10 h, and then obviously increased as time continued. With visible irradiation for 24 h, 82.1% of benzylamine was converted and >99% of them were selectively transformed to the corresponding imine, and the CO<sub>2</sub> was converted to CH<sub>3</sub>OH with high productivity up to 1017.7  $\mu\text{mol/g}$ , suggesting a satisfactory photocatalytic efficiency and selectivity under visible light conditions.

**Figure 6.** Cont.



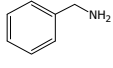
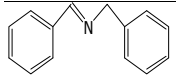
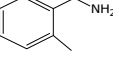
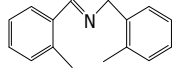
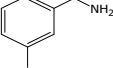
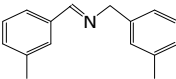
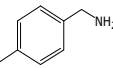
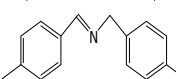
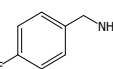
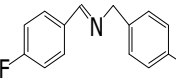
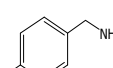
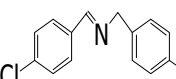
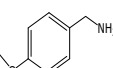
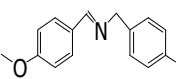
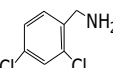
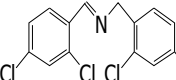
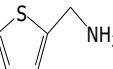
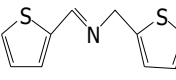
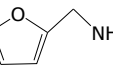
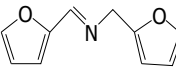

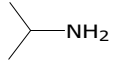
**Figure 6.** (a) Influence of irradiation time on conversion of benzylamine and selectivity of corresponding imine with  $\text{CuW}_{0.7}\text{Mo}_{0.3}\text{O}_4$  ( $x = 0.7$ ); (b) yields of  $\text{CH}_3\text{OH}$  production as a function of irradiation time.

Motivated by preceding results, the substrate scope of the oxidation of other amines to corresponding imines coupling with the reduction of  $\text{CO}_2$  to  $\text{CH}_3\text{OH}$  with photocatalytic  $\text{CuW}_{0.7}\text{Mo}_{0.3}\text{O}_4$  ( $x = 0.7$ ) was also carried out. Detailed results, shown in Table 3, show that the oxidative coupling reactions of the amine derivatives to their corresponding imines coupling with the formation of  $\text{CH}_3\text{OH}$  from  $\text{CO}_2$  could proceed well under the same conditions. However, different substrates can present great differences in the conversion of amines and the yield of  $\text{CH}_3\text{OH}$ . Methyl-substituted benzylamines at the *o*-, *m*-, and *p*- positions of the benzene ring (Table 3, entries 2–4) can also be converted, but there are slight differences in the conversion process, and it can be seen from the Table 3 that their conversion rates differ vary greatly, which might to be relative to the effect of the steric hindrance. It can be ascribed to the electronic effects associated with electron withdrawing substituents (entry 5–6) and electron donating substituents (entry 4,7) on the benzene ring have an obvious effect on the conversion rate of amines, as well as the yield of formation of  $\text{CH}_3\text{OH}$ . Two halo-substituted benzylamines could be oxidized to corresponding imines with a conversion of 30% and yield of 221.4  $\mu\text{mol/g}$  of  $\text{CH}_3\text{OH}$ . Moreover, heterocyclic amines were also transformed into the corresponding imines (entries 9–10). However, when aliphatic amines were selected as the substrates (Table 3, entry 11,12), no imines were obtained.

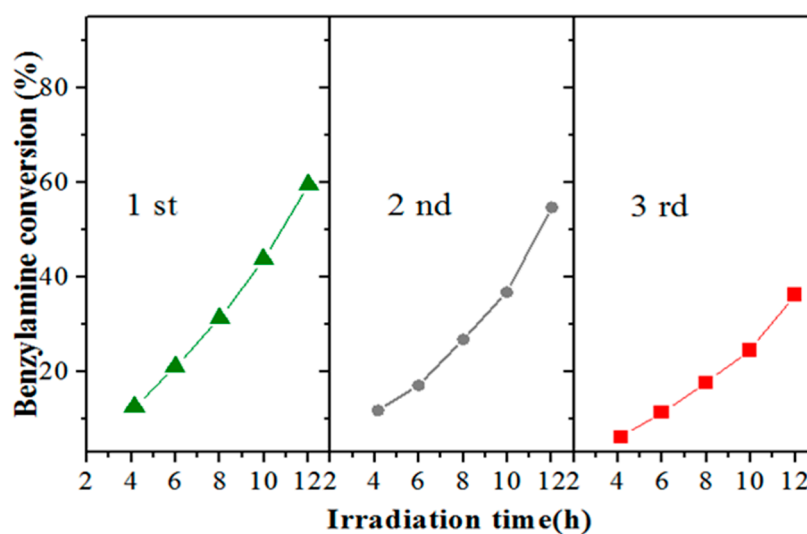
To measure the reusability of the photocatalyst, the  $\text{CuW}_{0.7}\text{Mo}_{0.3}\text{O}_4$  ( $x = 0.7$ ) was selected and re-used with the same reaction conditions three times. Before the proceeding reaction, the used photocatalysts were purified by thorough washing with  $\text{CH}_3\text{CN}$ . Figure 7 illustrates cycling runs of  $\text{CuW}_{0.7}\text{Mo}_{0.3}\text{O}_4$  ( $x = 0.7$ ) in the photocatalytic reduction of  $\text{CO}_2$  coupling with amine selective oxidation to imine under visible light irradiation. It is clear that the high photocatalytic activity of the as-prepared sample minimally decreased after three recycles, indicating good photocatalytic stability of the photocatalyst under visible light irradiation. The decrease in photocatalytic efficiency was mainly due to the loss of crystal water in the photocatalyst after use.



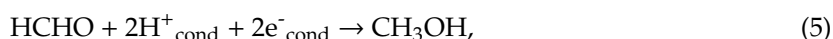
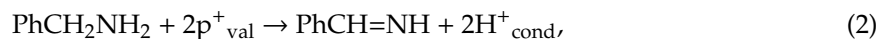
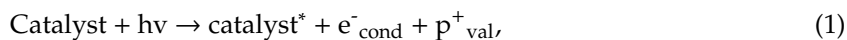
**Table 3.** <sup>a</sup> Effect of different amines on photocatalytic activity.

Entry	Reactant	Product	Yield <sup>b</sup>	Conv. (%) <sup>c</sup>	Sel. (%) <sup>d</sup>
1			671.8	57.2	99
2			127.5	16.3	99
3			227.4	26.2	98
4			251.9	43.9	99
5			33.1	6.5	98
6			137.2	19.4	98
7			214.6	25.1	99
8			221.4	30.6	99
9			126.2	16.3	98
10			29.7	4.9	98
11		—	—	—	—
12		—	—	—	—

<sup>a</sup> 1 mmol amine, 0.06 g photocatalysis, 40 mL CH<sub>3</sub>CN, 0.1 Mpa CO<sub>2</sub>; <sup>b</sup> Unit: (μmol g<sup>-1</sup>); <sup>c</sup> Conversion of amine; <sup>d</sup> Selectivity of the corresponding imine.

**Figure 7.** Photocatalytic activity of the reuse of CuW<sub>0.7</sub>Mo<sub>0.3</sub>O<sub>4</sub> (x = 0.7).

The mechanism for photocatalytic reduction of CO<sub>2</sub> to CH<sub>3</sub>OH coupling with the conversion of amine to corresponding imine is similar to our previous report [61] as shown in Figure 4. Details are as follows:



With absorption of visible light (Equations (1) and (2)), the photogenerated holes in the valence band (VB) of the photocatalyst oxidized benzylamine to the corresponding imine and generated H<sup>+</sup> (Equation (2)), which shows that CO<sub>2</sub> can be reduced by photoelectrons in conduction band (CB) to generate HCOOH, HCHO, and CH<sub>3</sub>OH (Equations (3)–(5)). The formed imine in Equation (2) was easily decomposed into benzaldehyde and NH<sub>3(S)</sub> (Equation (6)), and then the obtained benzaldehyde directly reacted with the benzylamine to form the corresponding imine and H<sub>2</sub>O (Equation (7)).

#### 4. Conclusions

In summary, a series of CuW<sub>x</sub>Mo<sub>(1-x)</sub>O<sub>4</sub> solid solutions were prepared and applied to the reduction of CO<sub>2</sub> into CH<sub>3</sub>OH coupling with the conversion of aromatic amine into its corresponding imine. The results revealed that the yield of CH<sub>3</sub>OH from CO<sub>2</sub> was 1017.7 μmol/g under 24 h visible light irradiations using an optimized photocatalyst, CuW<sub>0.7</sub>Mo<sub>0.3</sub>O<sub>4</sub> (x = 0.7). The catalyst chosen was associated with the maximum conversion (82.1%) of benzylamine to N-benzylidene benzylamine with high selectivity (>99%). Further experiments revealed that CuW<sub>0.7</sub>Mo<sub>0.3</sub>O<sub>4</sub> (x = 0.7) exhibited good substrate suitability, photocatalytic activity, and photocatalytic stability. All results should be helpful for the design and application of economical photocatalysts for the reduction of CO<sub>2</sub> to CH<sub>3</sub>OH under visible light.

**Supplementary Materials:** The following are available online at <http://www.mdpi.com/2079-4991/10/7/1303/s1>, Figure S1. GC chromatograms of (a) before irradiation and (b) the stand CH<sub>3</sub>OH and benzylamine in CH<sub>3</sub>CN and (c) product (CH<sub>3</sub>OH) after irradiation for 10 h with the partial enlarged drawing. Figure S2. The 1H NMR spectrums of (a) the product (CH<sub>3</sub>OH) photocatalyzed by CuW<sub>0.7</sub>Mo<sub>0.3</sub>O<sub>4</sub> (x = 0.7) after reaction for 10 h and (b) the stand CH<sub>3</sub>OH. Figure S3. the MS of Products photocatalyzed by CuW<sub>0.7</sub>Mo<sub>0.3</sub>O<sub>4</sub> (x = 0.7) after irradiation for 10 h. Figure S4. GC chromatograms of gas phase products after irradiation for 10 h. Figure S5. XPS spectra of (a) Cu<sub>2p</sub> and (b) W<sub>4f</sub> of photocatalysts.

**Author Contributions:** Writing—original draft, Writing—review & editing, C.L.; Data curation, T.Y., Q.H., and X.L.; Resources, H.L., and Y.Z.; Supervision, G.X., and W.Z.; Formal analysis, H.W. All authors have read and agreed to the published version of the manuscript.

**Funding:** This research received no external funding.

**Conflicts of Interest:** The authors declare no conflict of interest.

#### References

- Li, D.; Rohani, V.; Fabry, F.; Parakkulam Ramaswamy, A. Direct conversion of CO<sub>2</sub> and CH<sub>4</sub> into liquid chemicals by plasma-catalysis. *Appl. Catal. B Environ.* **2020**, *261*, 118228. [CrossRef]
- Wang, Y.; Gao, W.; Kazumi, S.; Li, H.; Yang, G.; Tsubaki, N. Direct and Oriented Conversion of CO<sub>2</sub> into Value-Added Aromatics. *Chemistry* **2019**, *25*, 5149–5153. [CrossRef]

3. Zheng, Y.; Vasileff, A.; Zhou, X.; Jiao, Y.; Jaroniec, M.; Qiao, S.-Z. Understanding the Roadmap for Electrochemical Reduction of CO<sub>2</sub> to Multi-Carbon Oxygenates and Hydrocarbons on Copper-Based Catalysts. *J. Am. Chem. Soc.* **2019**, *141*, 7646–7659. [[CrossRef](#)]
4. Ma, J.; Sun, N.; Zhang, X.; Zhao, N.; Xiao, F.; Wei, W.; Sun, Y. A short review of catalysis for CO<sub>2</sub> conversion. *Catal. Today* **2009**, *148*, 221–231. [[CrossRef](#)]
5. Hu, B.; Guild, C.; Suib, S.L. Thermal, electrochemical, and photochemical conversion of CO<sub>2</sub> to fuels and value-added products. *J. CO<sub>2</sub> Util.* **2013**, *1*, 18–27. [[CrossRef](#)]
6. Yang, S.; Rui, P.; Hensley, D.K.; Bonnesen, P.V.; Rondinone, A.J. High-Selectivity Electrochemical Conversion of CO<sub>2</sub> to Ethanol using a Copper Nanoparticle/N-doped Graphene Electrode. *Chemistryselect* **2016**, *1*, 6055–6061.
7. Benson, E.E.; Kubiak, C.P.; Sathrum, A.J.; Smieja, J.M. Electrocatalytic and homogeneous approaches to conversion of CO<sub>2</sub> to liquid fuels. *Chem. Soc. Rev.* **2008**, *38*, 89–99. [[CrossRef](#)]
8. Tu, W.; Yong, Z.; Zou, Z. ChemInform Abstract: Photocatalytic Conversion of CO<sub>2</sub> into Renewable Hydrocarbon Fuels: State-of-the-Art Accomplishment, Challenges, and Prospects. *Adv. Mater.* **2015**, *45*, 4607–4626.
9. Li, K.; An, X.; Park, K.H.; Khraisheh, M.; Tang, J. A critical review of CO<sub>2</sub> photoconversion: Catalysts and reactors. *Catal. Today* **2014**, *224*, 3–12. [[CrossRef](#)]
10. Lee, Y.Y.; Jung, H.S.; Kang, Y.T. A review: Effect of nanostructures on photocatalytic CO<sub>2</sub> conversion over metal oxides and compound semiconductors. *J. CO<sub>2</sub> Util.* **2017**, *20*, 163–177. [[CrossRef](#)]
11. Yuan, L.; Xu, Y.-J. Photocatalytic conversion of CO<sub>2</sub> into value-added and renewable fuels. *Appl. Surf. Sci.* **2015**, *342*, 154–167. [[CrossRef](#)]
12. Khalil, M.; Gunlazuardi, J.; Ivandini, T.A.; Umar, A. Photocatalytic conversion of CO<sub>2</sub> using earth-abundant catalysts: A review on mechanism and catalytic performance. *Renew. Sustain. Energy Rev.* **2019**, *113*, 109246. [[CrossRef](#)]
13. Das, S.; Daud, W.W. A review on advances in photocatalysts towards CO<sub>2</sub> conversion. *RSC Adv.* **2014**, *4*, 20856–20893. [[CrossRef](#)]
14. Roy, S.C.; Varghese, O.K.; Paulose, M.; Grimes, C.A. Toward Solar Fuels: Photocatalytic Conversion of Carbon Dioxide to Hydrocarbons. *ACS Nano* **2010**, *4*, 1259–1278. [[CrossRef](#)] [[PubMed](#)]
15. Xiong, Z.; Lei, Z.; Li, Y.; Dong, L.; Zhao, Y.; Zhang, J. A review on modification of facet-engineered TiO<sub>2</sub> for photocatalytic CO<sub>2</sub> reduction. *J. Photochem. Photobiol. C Photochem. Rev.* **2018**, *36*, 24–47. [[CrossRef](#)]
16. Zhao, H.; Pan, F.; Ying, L. A review on the effects of TiO<sub>2</sub> surface point defects on CO<sub>2</sub> photoreduction with H<sub>2</sub>O. *J. Mater.* **2016**, *3*, 17–32.
17. Shehzad, N.; Tahir, M.; Johari, K.; Murugesan, T.; Hussain, M. A critical review on TiO<sub>2</sub> based photocatalytic CO<sub>2</sub> reduction system: Strategies to improve efficiency. *J. CO<sub>2</sub> Util.* **2018**, *26*, 98–122. [[CrossRef](#)]
18. Cho, K.M.; Kim, K.H.; Park, K.; Kim, C.; Kim, S.; Al-Saggaf, A.; Gereige, I.; Jung, H.-T. Amine-functionalized graphene/CdS composite for photocatalytic reduction of CO<sub>2</sub>. *ACS Catal.* **2017**, *7*, 7064–7069. [[CrossRef](#)]
19. Jin, J.; Yu, J.; Guo, D.; Ho, W. A Hierarchical Z-Scheme CdS-WO<sub>3</sub> Photocatalyst with Enhanced CO<sub>2</sub> Reduction Activity. *Mater. Views* **2015**, *39*, 5262–5271.
20. Jin, J.; Tao, H. Facile synthesis of Bi<sub>2</sub>S<sub>3</sub> nanoribbons for photocatalytic reduction of CO<sub>2</sub> into CH<sub>3</sub>OH. *Appl. Surf. Sci.* **2016**, *394*, 364–370. [[CrossRef](#)]
21. Tran-Phu, T.; Daiyan, R.; Fusco, Z.; Ma, Z.; Amal, R.; Tricoli, A. Nanostructured β-Bi<sub>2</sub>O<sub>3</sub> Fractals on Carbon Fibers for Highly Selective CO<sub>2</sub> Electroreduction to Formate. *Adv. Functional Mater.* **2020**, *30*, 1906478. [[CrossRef](#)]
22. Liu, S.-Q.; Zhou, S.-S.; Chen, Z.-G.; Liu, C.-B.; Chen, F. An artificial photosynthesis system based on CeO<sub>2</sub> as light harvester and N-doped graphene Cu(II) complex as artificial metalloenzyme for CO<sub>2</sub> reduction to methanol fuel. *Catal. Commun.* **2016**, *73*, 7–11. [[CrossRef](#)]
23. Li, M.; Zhang, L.; Wu, M.; Du, Y.; Fan, X.; Wang, M.; Zhang, L.; Kong, Q.; Shi, J. Mesoporous CeO<sub>2</sub>/g-C<sub>3</sub>N<sub>4</sub> nanocomposites: Remarkably enhanced photocatalytic activity for CO<sub>2</sub> reduction by mutual component activations. *Nano Energy* **2016**, *19*, 145–155. [[CrossRef](#)]
24. Zhou, Y.; Tian, Z.; Zhao, Z.; Liu, Q.; Kou, J.; Chen, X.; Gao, J.; Yan, S.; Zou, Z. High-Yield Synthesis of Ultrathin and Uniform Bi<sub>2</sub>WO<sub>6</sub> Square Nanoplates Benefitting from Photocatalytic Reduction of CO<sub>2</sub> into Renewable Hydrocarbon Fuel under Visible Light. *ACS Appl Mater Interfaces* **2011**, *3*, 3594–3601. [[CrossRef](#)]

25. Dai, W.; Xu, H.; Yu, J.; Hu, X.; Luo, X.; Tu, X.; Yang, L. Photocatalytic reduction of CO<sub>2</sub> into methanol and ethanol over conducting polymers modified Bi<sub>2</sub>WO<sub>6</sub> microspheres under visible light. *Appl. Surf. Sci.* **2015**, *356*, 173–180. [[CrossRef](#)]
26. Xiao, L.; Lin, R.; Wang, J.; Cui, C.; Wang, J.; Li, Z. A Novel Hollow-Hierarchical Structured Bi<sub>2</sub>WO<sub>6</sub> with Enhanced Photocatalytic Activity for CO<sub>2</sub> Photoreduction. *J. Colloid Interface Sci.* **2018**, *523*, 151–158. [[CrossRef](#)]
27. Wang, J.C.; Zhang, L.; Fang, W.X.; Ren, J.; Li, Z. Enhanced Photoreduction CO<sub>2</sub> Activity over Direct Z-Scheme α-Fe<sub>2</sub>O<sub>3</sub>/Cu<sub>2</sub>O Heterostructures Under Visible Light Irradiation. *ACS Appl. Mater. Interfaces* **2015**, *7*, 8631–8639. [[CrossRef](#)]
28. Guo, Z.; Fei, Y.; Ying, Y.; Leung, C.F.; Ng, S.M.; Ko, C.C.; Cometto, C.; Lau, T.C.; Robert, M. Photocatalytic Conversion of CO<sub>2</sub> to CO by a Copper(II) Quaterpyridine Complex. *ChemSuschem* **2017**, *10*, 4009–4013. [[CrossRef](#)]
29. Niu, K.; Xu, Y.; Wang, H.; Ye, R.; Xin, H.L.; Lin, F.; Tian, C.; Lum, Y.; Bustillo, K.C.; Doeff, M.M. A spongy nickel-organic CO<sub>2</sub> reduction photocatalyst for nearly 100% selective CO production. *Sci. Adv.* **2017**, *3*, e1700921. [[CrossRef](#)]
30. Wu, T.; Zou, L.; Han, D.; Li, F.; Zhang, Q.; Niu, L. A carbon-based photocatalyst efficiently converts CO<sub>2</sub> to CH<sub>4</sub> and C<sub>2</sub>H<sub>2</sub> under visible light. *Green Chem.* **2014**, *16*, 2142. [[CrossRef](#)]
31. Xiong, Z.; Lei, Z.; Kuang, C.C.; Chen, X.; Gong, B.; Zhao, Y.; Zhang, J.; Zheng, C.; Wu, J.C.S. Selective photocatalytic reduction of CO<sub>2</sub> into CH<sub>4</sub> over Pt-Cu<sub>2</sub>O TiO<sub>2</sub> nanocrystals: The interaction between Pt and Cu<sub>2</sub>O cocatalysts. *Appl. Catal. B Environ.* **2016**, *202*, 695–703. [[CrossRef](#)]
32. Li, H.; Gao, Y.; Xiong, Z.; Liao, C.; Shih, K. Enhanced selective photocatalytic reduction of CO<sub>2</sub> to CH<sub>4</sub> over plasmonic Au modified g-C<sub>3</sub>N<sub>4</sub> photocatalyst under UV-vis light irradiation. *Appl. Surf. Sci.* **2018**, *439*, 552–559. [[CrossRef](#)]
33. Chen, J.; Xin, F.; Niu, H.; MAo, C.-j.; Song, J.-M. Photocatalytic reduction of CO<sub>2</sub> with methanol over Bi<sub>2</sub>S<sub>3</sub>-ZnIn<sub>2</sub>S<sub>4</sub> nanocomposites. *Mater. Lett.* **2017**, *198*, 1–3. [[CrossRef](#)]
34. Yu, W.; Xu, D.; Peng, T. Enhanced photocatalytic activity of g-C<sub>3</sub>N<sub>4</sub> for selective CO<sub>2</sub> reduction to CH<sub>3</sub>OH via facile coupling of ZnO: A direct Z-scheme mechanism. *J. Mater. Chem. A* **2015**, *3*, 19936. [[CrossRef](#)]
35. Phongamwong, T.; Chareonpanich, M.; Limtrakul, J. Role of chlorophyll in Spirulina on photocatalytic activity of CO<sub>2</sub> reduction under visible light over modified N-doped TiO<sub>2</sub> photocatalysts. *Appl. Catal. B Environ.* **2014**, *168–169*, 114–124.
36. Lo, C.C.; Hung, C.-H.; Yuan, C.-S.; Wu, J.-F. Photoreduction of carbon dioxide with H<sub>2</sub> and H<sub>2</sub>O over TiO<sub>2</sub> and ZrO<sub>2</sub> in a circulated photocatalytic reactor. *Sol. Energy Mater. Sol. Cells* **2007**, *91*, 1765–1774. [[CrossRef](#)]
37. Wang, J.; Li, G.; Li, Z.; Tang, C.; Feng, Z.; An, H.; Liu, H.; Liu, T.; Li, C. A highly selective and stable ZnO-ZrO<sub>2</sub> solid solution catalyst for CO<sub>2</sub> hydrogenation to methanol. *Sci. Adv.* **2017**, *3*, e1701290. [[CrossRef](#)]
38. Maeda, K.; Teramura, L.; Takata, T.; Hara, M.; Saito, N.; Toda, K.; Inoue, Y.; Hisayoshi, K.; Domen, K. Overall Water Splitting on (Ga<sub>1-x</sub>Zn<sub>x</sub>)(N<sub>1-x</sub>O<sub>x</sub>) Solid Solution Photocatalyst: Relationship between Physical Properties and Photocatalytic Activity. *J. Phys. Chem. B* **2005**, *109*, 20504–20510. [[CrossRef](#)] [[PubMed](#)]
39. Yan, S.; Wang, J.; Gao, H.; Wang, N.; Yu, H.; Li, Z.; Zhou, Y.; Zou, Z. Zinc Gallogermanate Solid Solution: A Novel Photocatalyst for Efficiently Converting CO<sub>2</sub> into Solar Fuels. *Adv. Funct. Mater.* **2013**, *23*, 1839–1845. [[CrossRef](#)]
40. Chai, Y.; Li, L.; Lu, J.; Li, D.; Shen, J.; Zhang, Y.; Liang, J.; Wang, X. Germanium-substituted Zn<sub>2</sub>TiO<sub>4</sub> solid solution photocatalyst for conversion of CO<sub>2</sub> into fuels. *J. Catal.* **2019**, *371*, 144–152. [[CrossRef](#)]
41. Ohno, T.; Bai, L.; Hisatomi, T.; Maeda, K.; Domen, K. Photocatalytic Water Splitting Using Modified GaN:ZnO Solid Solution under Visible Light: Long-Time Operation and Regeneration of Activity. *J. Am. Chem. Soc.* **2012**, *134*, 8254–8259. [[CrossRef](#)] [[PubMed](#)]
42. Li, Z.; Zhang, F.; Han, J.; Zhu, J.; Li, M.; Zhang, B.; Fan, W.; Lu, J.; Li, C. Using Pd as a Cocatalyst on GaN-ZnO Solid Solution for Visible-Light-Driven Overall Water Splitting. *Catal. Lett.* **2018**, *148*, 933–939. [[CrossRef](#)]
43. Maeda, K.; Takata, T.; Hara, M.; Saito, N.; Inoue, Y.; Kobayashi, H.; Domen, K. GaN:ZnO Solid Solution as a Photocatalyst for Visible-Light-Driven Overall Water Splitting. *J. Am. Chem. Soc.* **2006**, *127*, 8286–8287. [[CrossRef](#)] [[PubMed](#)]
44. Yu, X.; Shavel, A.; An, X.; Luo, Z.; Ibáñez, M.; Cabot, A. Cu<sub>2</sub>ZnSnS<sub>4</sub>-Pt and Cu<sub>2</sub>ZnSnS<sub>4</sub>-Au Heterostructured Nanoparticles for Photocatalytic Water Splitting and Pollutant Degradation. *J. Am. Chem. Soc.* **2014**, *136*, 9236–9239. [[CrossRef](#)] [[PubMed](#)]

45. Qi, L.; Yang, Y.; Zhang, P.; Le, Y.; Wang, C.; Wu, T. Hierarchical flower-like BiOI<sub>x</sub>Br<sub>(1-x)</sub> solid solution spheres with enhanced visible-light photocatalytic activity. *Appl. Surf. Sci.* **2019**, *467–468*, 792–801. [[CrossRef](#)]
46. Ouyang, S.; Ye, J.  $\beta$ -AgAl<sub>(1-x)</sub>Ga<sub>(x)</sub>O<sub>2</sub> solid-solution photocatalysts: Continuous modulation of electronic structure toward high-performance visible-light photoactivity. *J. Am. Chem. Soc.* **2011**, *133*, 7757. [[CrossRef](#)] [[PubMed](#)]
47. Gao, M.; Yang, J.; Sun, T.; Zhang, Z.; Zhang, D.; Huang, H.; Lin, H.; Fang, Y.; Wang, X. Persian buttercup-like BiOBr<sub>x</sub>Cl<sub>1-x</sub> solid solution for photocatalytic overall CO<sub>2</sub> reduction to CO and O<sub>2</sub>. *Appl. Catal. B Environ.* **2019**, *243*, 734–740. [[CrossRef](#)]
48. Pan, L.; Xuehua, Z.; Chun-Chao, H.; Lin, L.; Chen, Y.; Tao, H. Visible-light driven CO<sub>2</sub> photoreduction over Zn<sub>x</sub>Cd<sub>1-x</sub>S solid solution coupling with tetra(4-carboxyphenyl)porphyrin iron(III) chloride. *Phys. Chem. Chem. Phys.* **2018**, *20*, 16985.
49. Zhou, P.; Wang, X.; Yan, S.; Zou, Z. Solid Solution Photocatalyst with Spontaneous Polarization Exhibiting Low Recombination Toward Efficient CO<sub>2</sub> Photoreduction. *Chemsuschem* **2016**, *9*, 2064–2068. [[CrossRef](#)] [[PubMed](#)]
50. Liu, J.Y.; Garg, B.; Ling, Y.-C. Cu<sub>x</sub>Ag<sub>y</sub>In<sub>z</sub>Zn<sub>k</sub>S<sub>m</sub> solid solutions customized with RuO<sub>2</sub> or Rh<sub>1.32</sub>Cr<sub>0.66</sub>O<sub>3</sub> co-catalyst display visible light-driven catalytic activity for CO<sub>2</sub> reduction to CH<sub>3</sub>OH. *Green Chem.* **2011**, *13*, 2029. [[CrossRef](#)]
51. Liang, J.; Li, L. Synthesis of N-doped graphene-functionalized Zn<sub>1.231</sub>Ge<sub>0.689</sub>N<sub>1.218</sub>O<sub>0.782</sub> solid solution as a photocatalyst for CO<sub>2</sub> reduction and oxidation of benzyl alcohol under visible-light irradiation. *J. Mater. Chem. A* **2017**, *5*, 10998. [[CrossRef](#)]
52. Benko, F.A.; MacLaurin, C.L.; Koffyberg, F.P. CuWO<sub>4</sub> and Cu<sub>3</sub>WO<sub>6</sub> as anodes for the photoelectrolysis of water. *Mater. Res. Bull.* **1982**, *17*, 133–136. [[CrossRef](#)]
53. Lhermitte, C.R.; Bartlett, B.M. Advancing the Chemistry of CuWO<sub>4</sub> for Photoelectrochemical Water Oxidation. *Acc. Chem. Res.* **2016**, *49*, 1121–1129. [[CrossRef](#)] [[PubMed](#)]
54. Cheng, J.; Lei, C.; Xiong, E.; Jiang, Y.; Xia, Y. Preparation and characterization of W–Cu nanopowders by a homogeneous precipitation process. *J. Alloy. Compd.* **2006**, *421*, 146–150. [[CrossRef](#)]
55. Azar, G.T.P.; Rezaie, H.R.; Razavizadeh, H. Synthesis and consolidation of W–Cu composite powders with silver addition. *Int. J. Refract. Met. Hard Mater.* **2012**, *31*, 157–163. [[CrossRef](#)]
56. Calvert, L.D.; Barnes, W.H. The structure of lindgrenite. *Can Miner.* **1957**, *6*, 31–51.
57. Fu, X.; Ji, J.; Tang, W.; Liu, W.; Chen, S. Mo–W based copper oxides: Preparation, characterizations, and photocatalytic reduction of nitrobenzene. *Mater. Chem. Phys.* **2013**, *141*, 719–726. [[CrossRef](#)]
58. Gaudon, M.; Carbonera, C.; Thiry, A.E.; Demourgues, A.; Deniard, P.; Payen, C.; Létard, J.F.; Jobic, S. Adaptable Thermochromism in the CuMo 1-x W x O 4 Series (0 ≤ x < 0.1): A Behavior Related to a First-Order Phase Transition with a Transition Temperature Depending on x. *Inorg. Chem.* **2007**, *46*, 10200–10207.
59. Jing, L.; Qu, Y.; Wang, B.; Li, S.; Jiang, B.; Yang, L.; Fu, W.; Fu, H.; Sun, J. Review of photoluminescence performance of nano-sized semiconductor materials and its relationships with photocatalytic activity. *Sol. Energy Mater. Sol. Cells* **2006**, *90*, 1773–1787.
60. Yu, J.-G.; Yu, H.-G.; Cheng, B.; Zhao, X.-J.; Yu, J.C.; Ho, W.-K. The Effect of Calcination Temperature on the Surface Microstructure and Photocatalytic Activity of TiO<sub>2</sub> Thin Films Prepared by Liquid Phase Deposition. *J. Phys. Chem. B* **2003**, *107*, 13871–13879. [[CrossRef](#)]
61. Yang, T.; Yu, Q.; Wang, H. Photocatalytic Reduction of CO<sub>2</sub> to CH<sub>3</sub>OH Coupling with the Oxidation of Amine to Imine. *Catal. Lett.* **2018**, *148*, 2382–2390. [[CrossRef](#)]

